Supporting Information

Multi-functionalized carbon nanotubes towards green fabrication of heterogeneous catalyst platforms with enhanced catalytic properties under NIR light irradiation

Xuefeng Pan[a,d†], Rongying Liu[b†], Zhilong Yu[a], Benedikt Haas[c], Zdravko Kochovski[a], Sijia Cao[a,d], Radwan M. Sarhan[a], Guosong Chen[b], and Yan Lu[a,d]**

[a] *Department for Electrochemical Energy Storage, Helmholtz-Zentrum Berlin für Materialien und Energie, Hahn-Meitner-Platz 1, 14109 Berlin, Germany*

[b] *The State Key Laboratory of Molecular Engineering of Polymers and Department of Macromolecular Science, Fudan University, Shanghai 200433, China*

[c] *Department of Physics & IRIS Adlershof, Humboldt-Universität zu Berlin, Newtonstr. 15, 12489 Berlin, Germany*

[d] *Institute of Chemistry, University of Potsdam, Karl-Liebknecht-Str. 24-25, 14476 Potsdam, Germany*

[†] These two authors contribute equally to this manuscript.

** Corresponding authors:*

Guosong Chen: guosong@fudan.edu.cn

Yan Lu: yan.lu@helmholtz-berlin.de

Supplementary data

Supplementary Figures

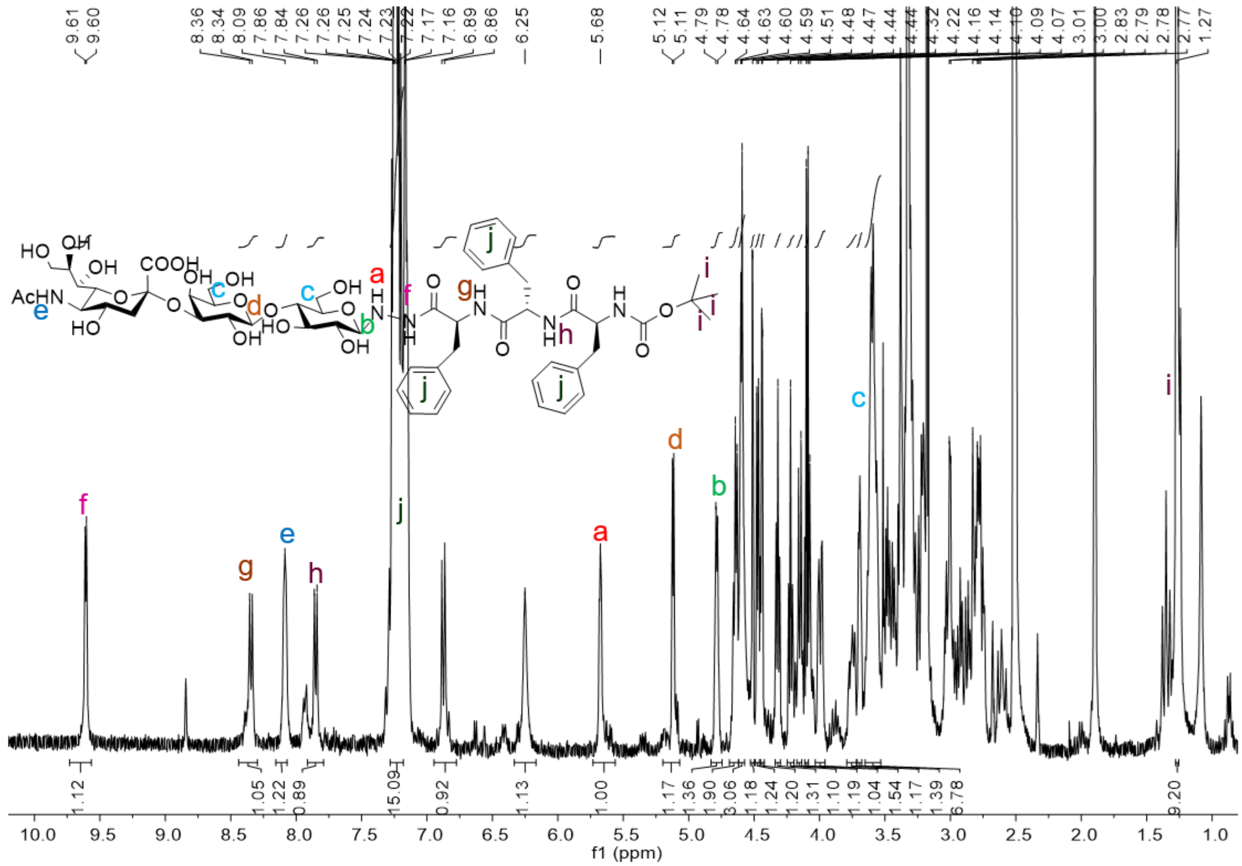

Fig. S1. ¹H-NMR spectrum of the GP powder dissolved in DMSO-*d6***.**

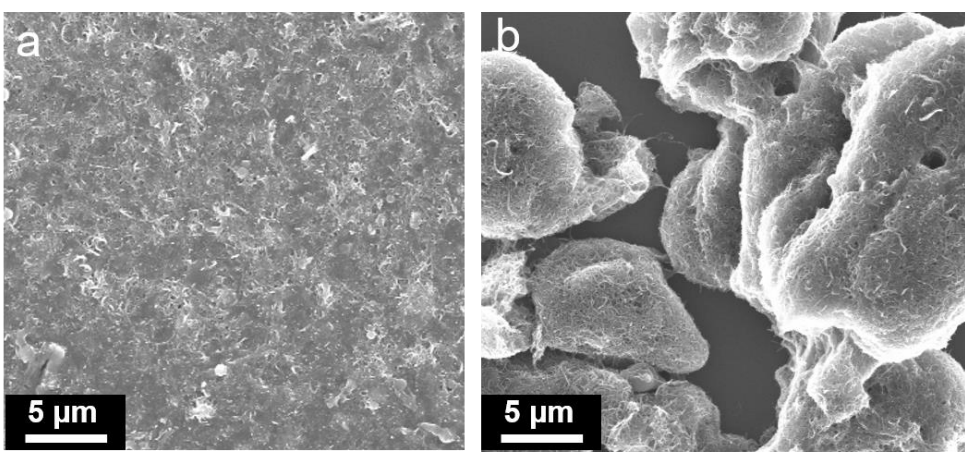

Fig. S2. SEM images of (a) the GP-CNTs dispersion and (b) the pristine CNTs cluster with a scale bar of 5 µm**.**

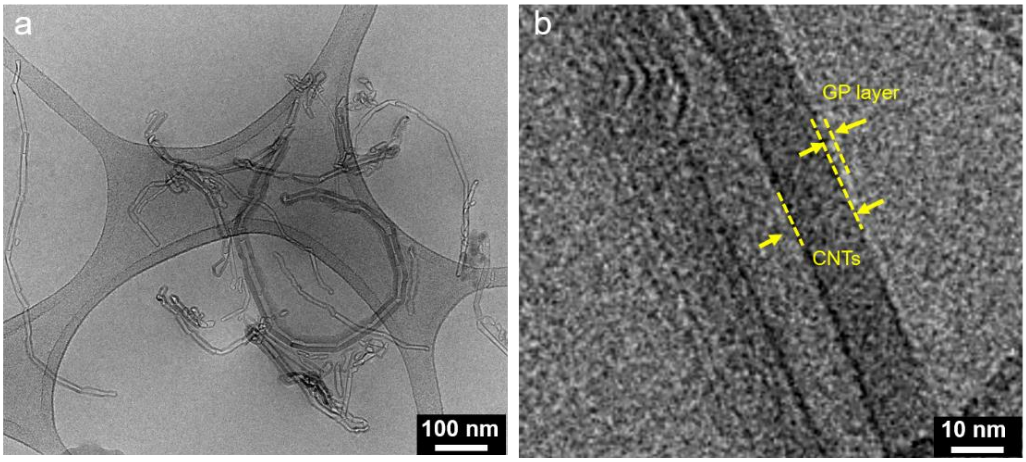

Fig. S3. Cryo-TEM images of the GP-CNTs dispersion at different magnifications.

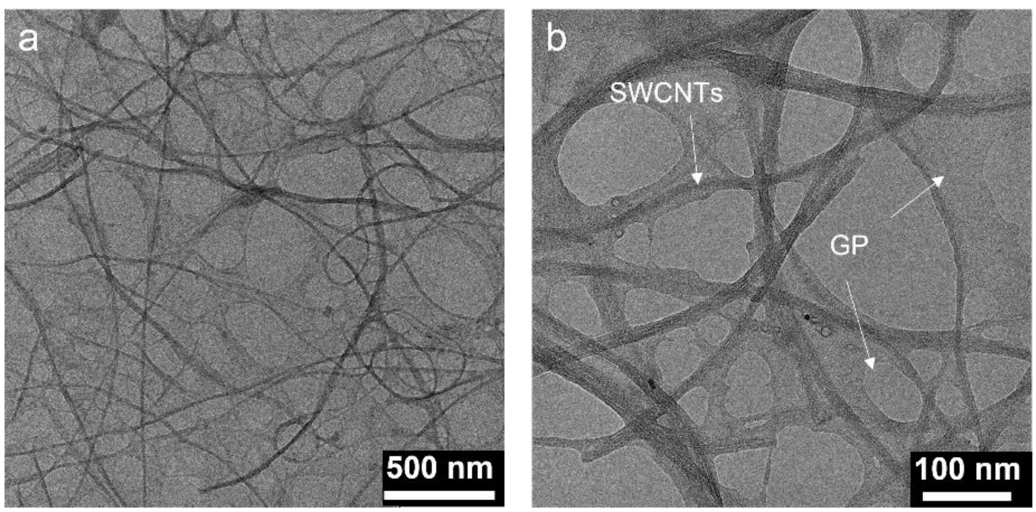

Fig. S4. TEM images of the SWCNTs dispersed with GP (same mass ratio of 1:1) at different magnifications.

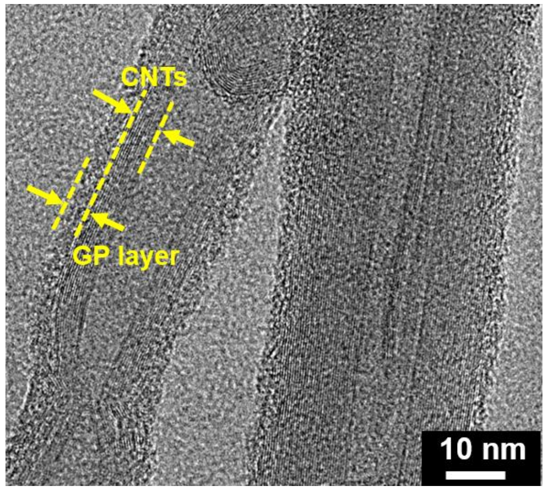

Fig. S5. HRTEM image of the GP-CNTs dispersion after storage for 2 months.

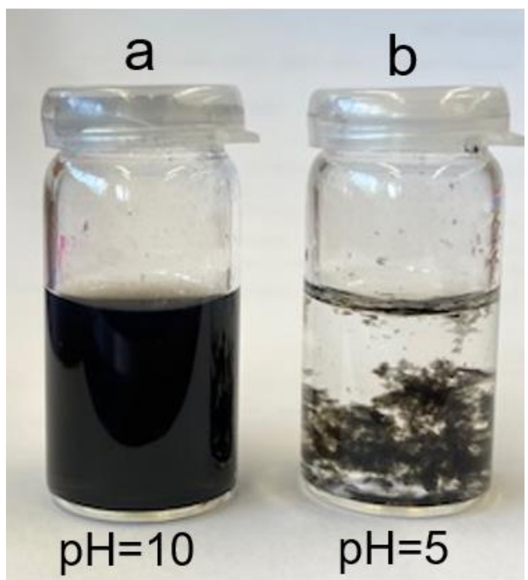

Fig. S6. Photos of the GP-CNTs dispersions at 0.2 mg/mL and the pH of (a) 10 and (b) 5 overnight.

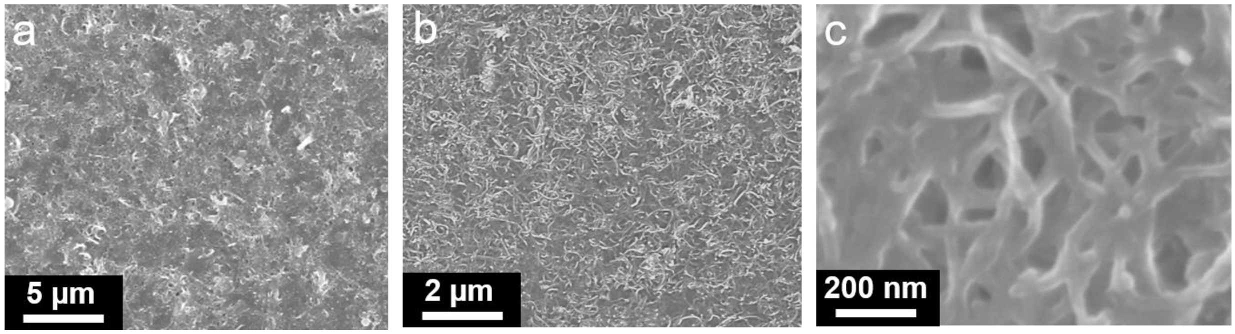

Fig. S7. SEM images of the GP-CNTs film after drying at various magnifications.

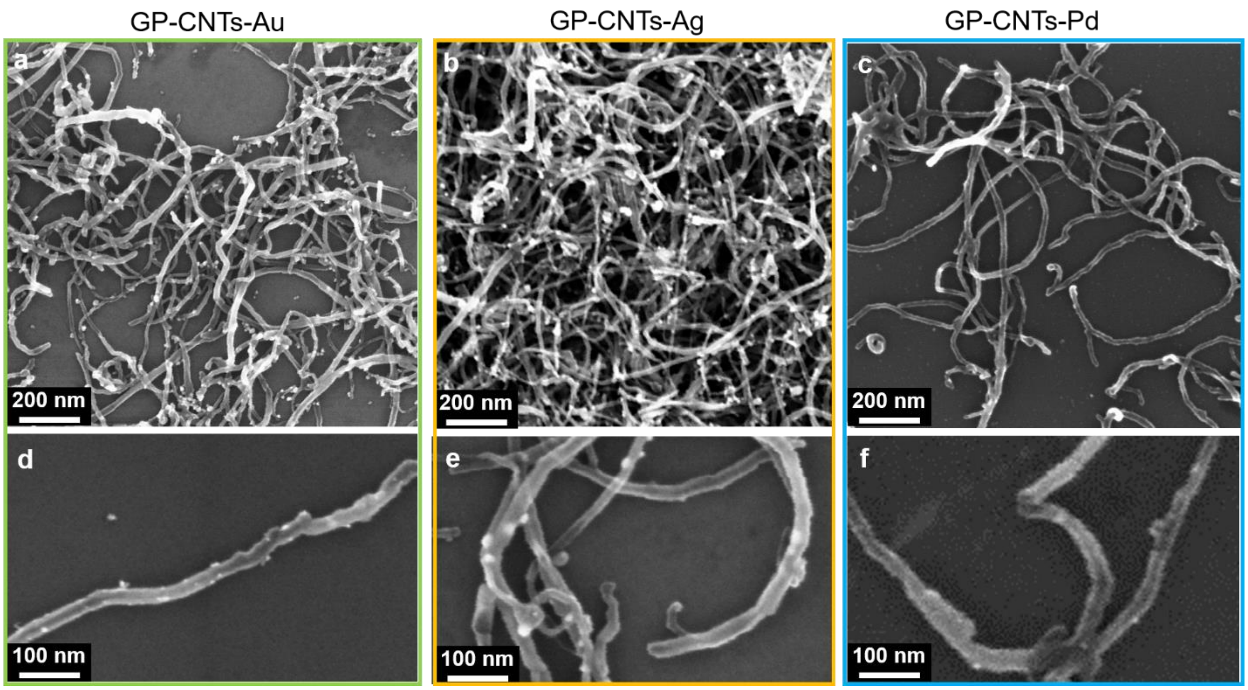

Fig. S8. SEM images of (a) GP-CNTs-Au, (b) GP-CNTs- Ag, and (c) GP-CNTs-Pd.

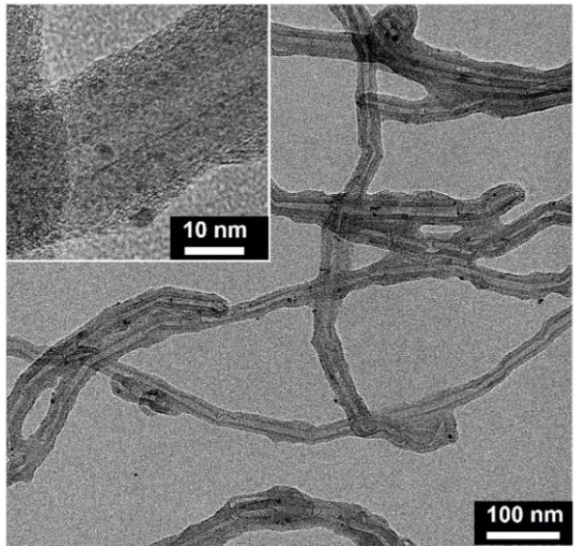

Fig. S9. TEM images of the GP-CNTs-Pd sample after storage for 1 month.

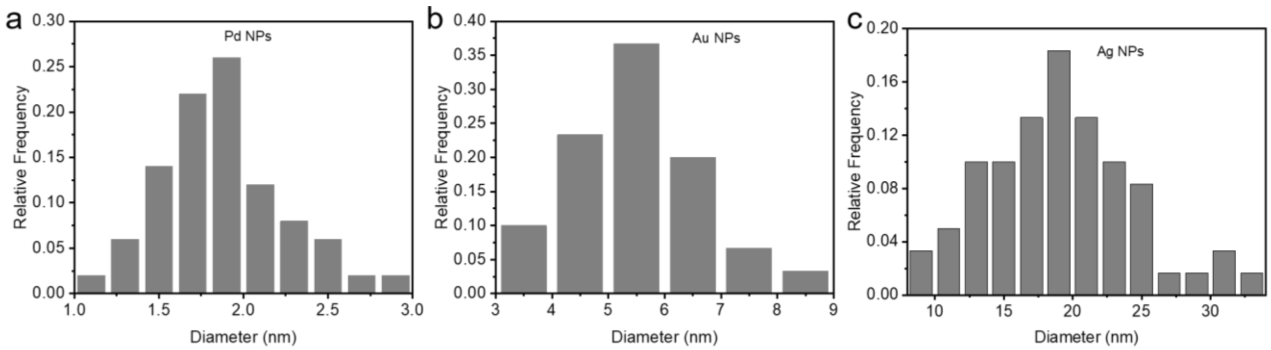

Fig. S10. Histograms of particle size distribution (based on over 50 particles) of (a) Pd NPs in GP-CNTs-Pd, (b) Au NPs in GP-CNTs-Au, and (c) Ag NPs in GP-CNTs-Ag determined from TEM analysis based on more than 50 particles.

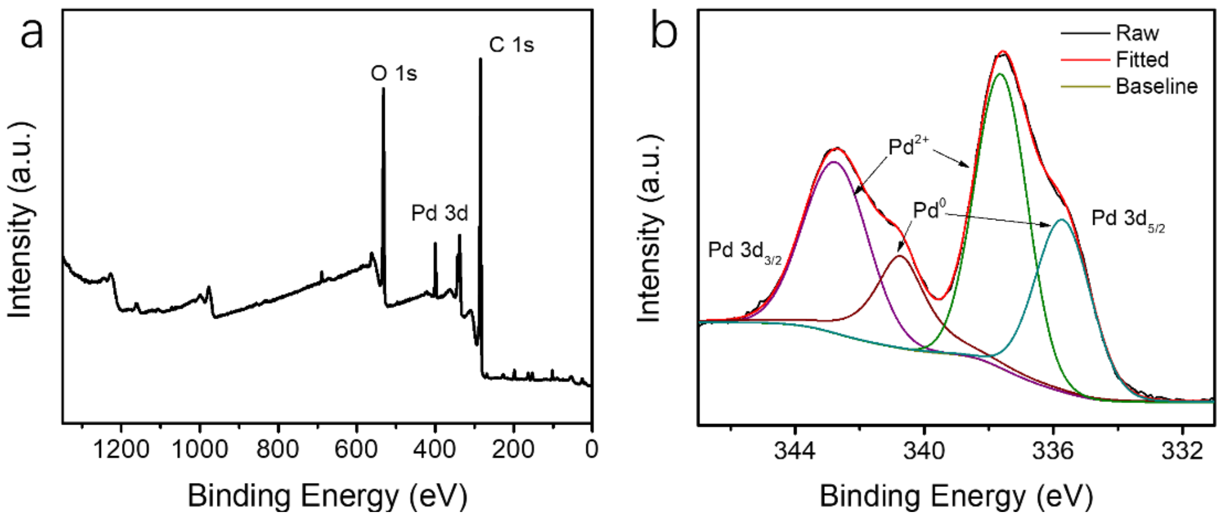

Fig. S11. (a) Full XPS spectrum and (b) high-resolution Pd 3d spectrum of the GP-CNTs-Pd composite.

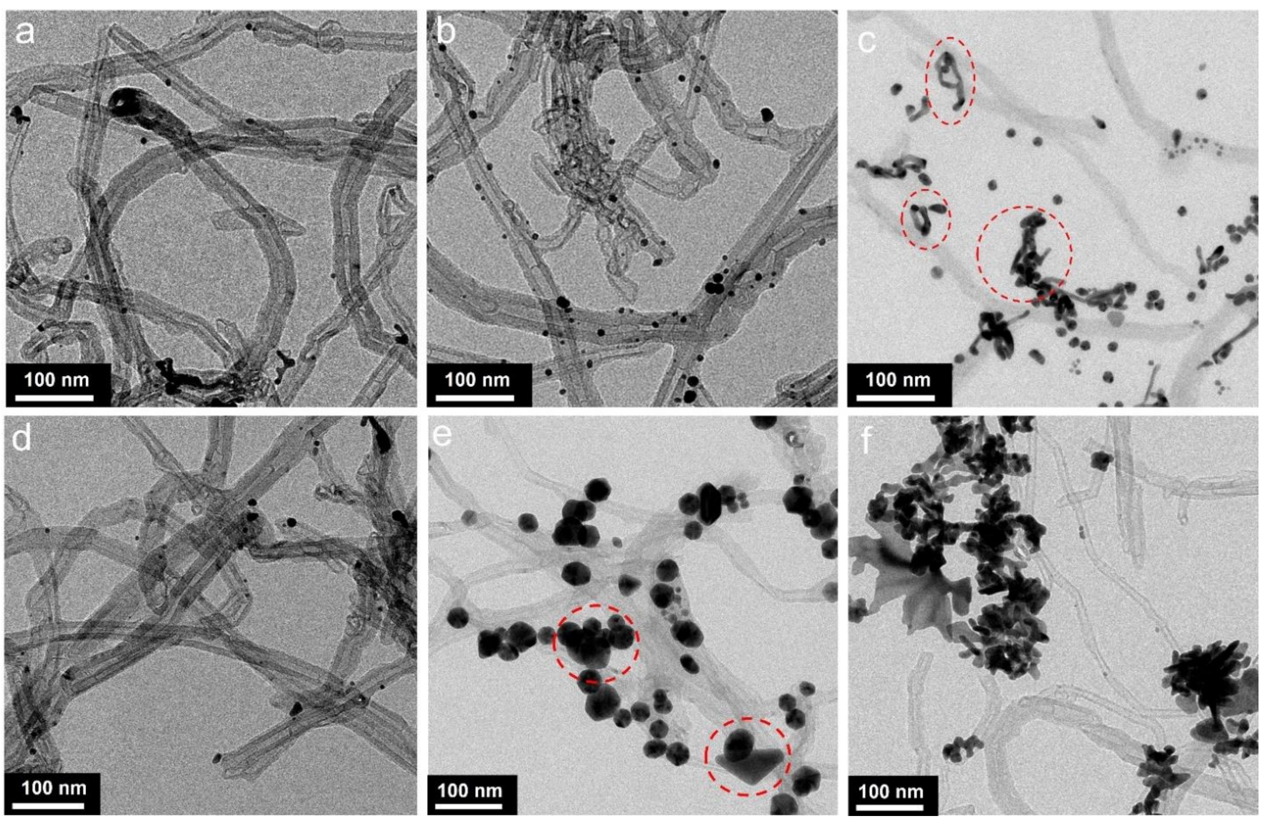

Fig. S12. TEM images of GP-CNTs-Au prepared at (a) 0.02 mg/mL of GP, 0.15 mM of $HAuCl_4$; (b) 0.05 mg/mL of GP, 0.15 mM of $HAuCl_4$; (c) 0.1 mg/mL of GP, 0.15 mM of $HAuCl_4$; (d) 0.05 mg/mL of GP, 0.05 mM of $HAuCl_4$; (e) 0.05 mg/mL of GP, 0.3 mM of $HAuCl_4$; and (f) 0.05 mg/mL of GP, 0.15 mM of $HAuCl_4$ heated at 40 °C. Note that all the samples in (a-e) were prepared at room temperature.

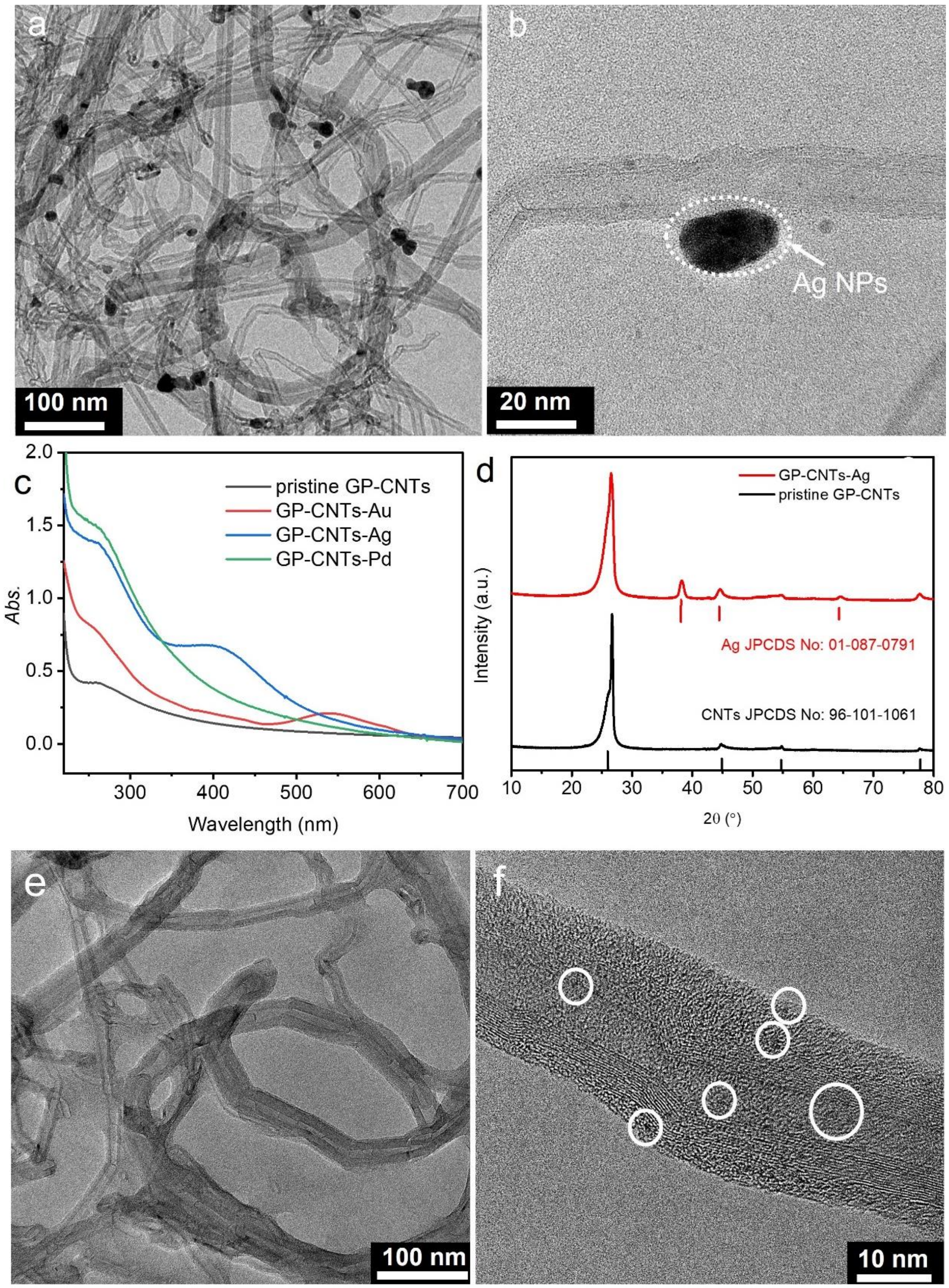

Fig. S13. (a, b) TEM images of GP-CNTs-Ag at different magnifications. (c) UV-Vis absorption spectra of various metal/CNTs composites. (d) XRD patterns of the pristine GP-CNTs and GP-CNTs-Ag powder after freeze-drying. The peaks at 38.2, 44.3, and 64.7° in XRD indicate the (111), (200), and (220) planes of the (*fcc*) metallic Ag (JPCDS NO. 01-087-0719).[1] (e-f) TEM images of the GP-CNTs-Pt prepared by mixing GP-CNTs (0.05 mg/mL) with H_2PtCl_6 (0.15 mM) at room temperature with stirring for 24 h.

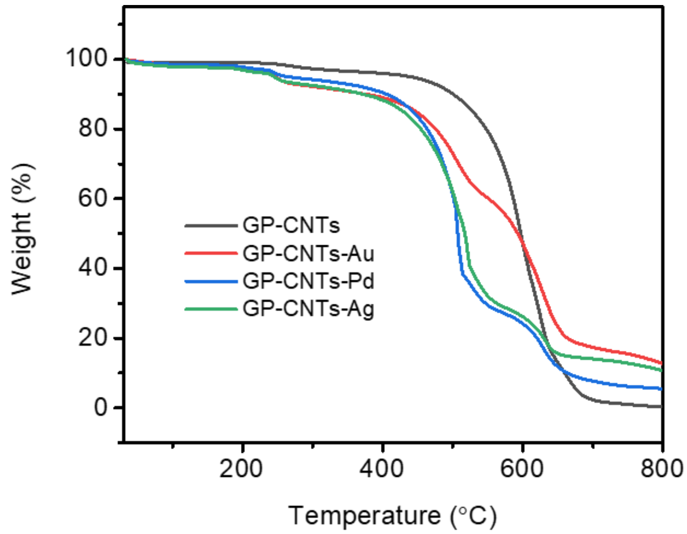

Fig. S14. TGA curves of the GP-CNTs-Au, GP-CNTs-Ag, and GP-CNTs-Pd powder in synthetic air.

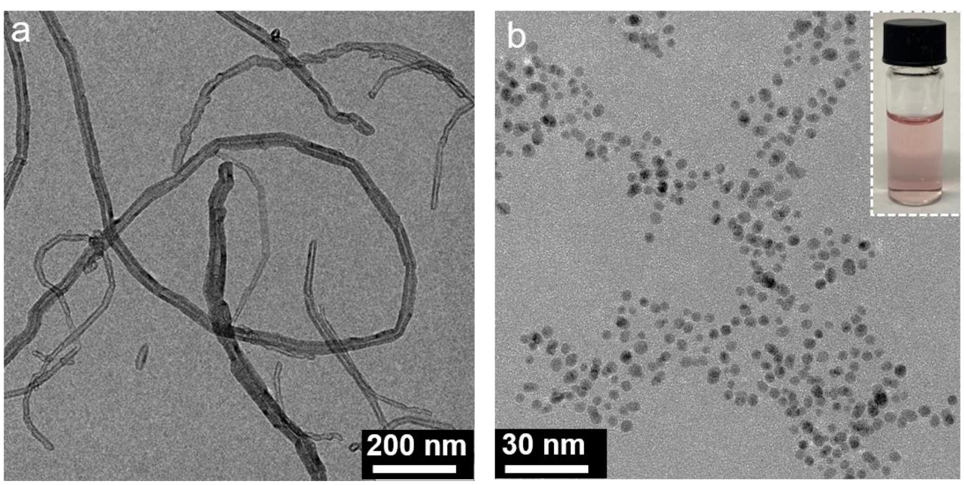

Fig. S15. TEM images of (a) Pristine CNTs cluster mixed with $HAuCl_4$ in the absence of GP molecules. (b) Au NPs generated in the mixture of $HAuCl_4$ (0.01 mM) and GP (0.1 mg/mL) solution. The inset in (b) is the corresponding photo of the obtained Au NPs dispersion.

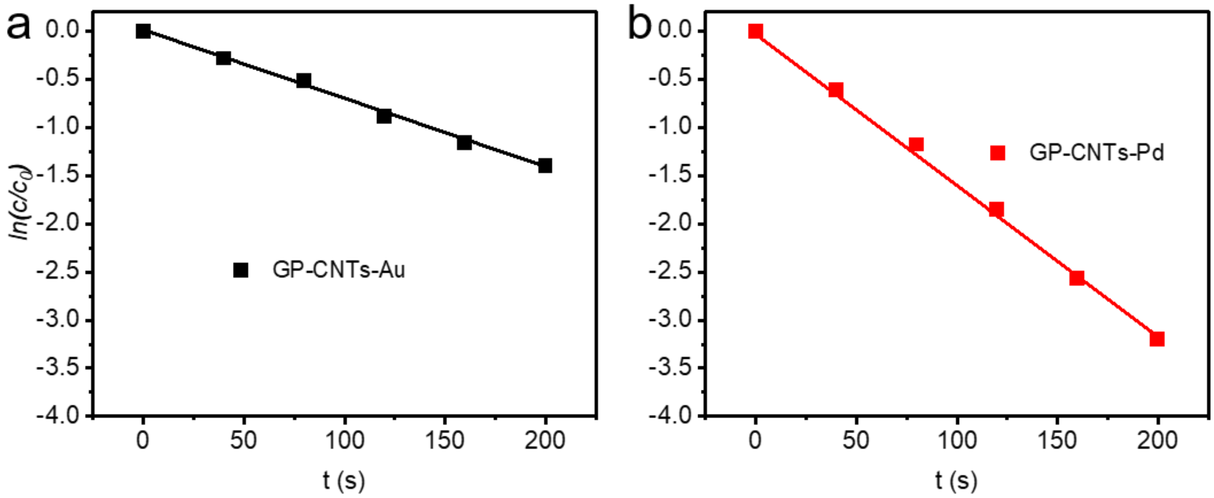

Fig. S16. Reduction of 4-NP with (a) GP-CNTs-Au at 10.5 μg/mL and (b) GP-CNTs-Pd at 1.80 μg/mL. The concentration of 4-NP and $NaBH_4$ was 0.005 mM and 0.1 M, respectively.

When adding an excess amount of $NaBH_4$, the reduction kinetics of 4-NP mainly follow a pseudo-first-order law. Apparent rate constant (k_{app}) of 4-NP can be given by:

$$ln\frac{c}{c_0} = ln\frac{I}{I_0} = -k_{app}t = -k_1 S_t t \quad (1)$$

where c and c_0 are the concentration and I and I_0 are the absorption intensity at 400 nm of 4-NP at the given time t and the very beginning of the reaction, respectively.[2] S_t is the total surface of catalytic particle and k_1 is the rate constant normalized to S_t. k_{app} can be obtained from the linear correlation between $ln(I/I_0)$ or $ln(c/c_0)$ and t. As a result, GP-CNTs-Pd displayed a fast catalytic conversion of 4-NP, giving a k_{app} value of 0.016 s^{-1}, while a k_{app} value of 0.0021 s^{-1} has been measured for GP-CNTs-Au (Fig. S16).

Note that the reduction mainly proceeds on the surface of the metal NPs. If we assume both Pd and Au particles are ideally spherical, S_t can be thus calculated by:

$$m_0 = \frac{1}{6}\rho\pi d^3 \quad (2)$$

$$S_0 = \pi d^2 \quad (3)$$

$$n = \frac{m}{m_0} \quad (4)$$

$$S_t = \frac{nS_0}{V} \quad (5)$$

where m_0 S_0, and n are the mass and surface of a single catalyst particle and the total number of metal particles, respectively; m is the total mass of metal catalyst that can be estimated from TGA measurement (13.2 wt.% for GP-CNTs-Pd and 11.5 wt.% for GP-CNTs-Au); ρ is the density of the catalytic particle, assuming it is the same as the density of their bulk material (12.0 g/cm^3 for Pd and 19.3 g/cm^3 for Au); d is the diameter of the particle, which can be obtained from the HRTEM analysis (1.8 nm for Pd and 5.6 nm for Au).[3] V is the reaction volume (2.5 mL here). According to Table S2, the S_t was thereby fixed to be 0.26 m^2/L. The value of GP-CNTs-Pd was calculated to be 0.062 s^{-1} m^{-2} L, which is higher than that of GP-CNTs-Au (0.0081 s^{-1} m^{-2} L), demonstrating the superior catalytic activity of GP-CNTs-Pd.

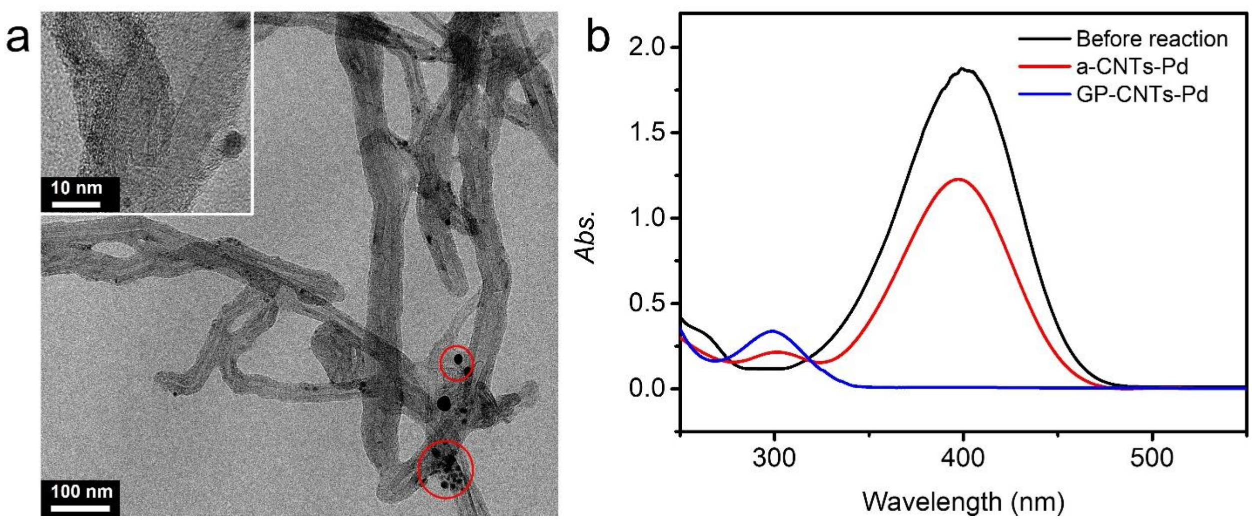

Fig. S17. (a) TEM images of a-CNTs-Pd. (b) Reaction comparison: both a-CNTs-Pd and GP-CNTs-Pd at the concentration of 0.02 mg/mL, 4-NP at 0.1 mM, and $NaBH_4$ at 20 mM at room temperature.

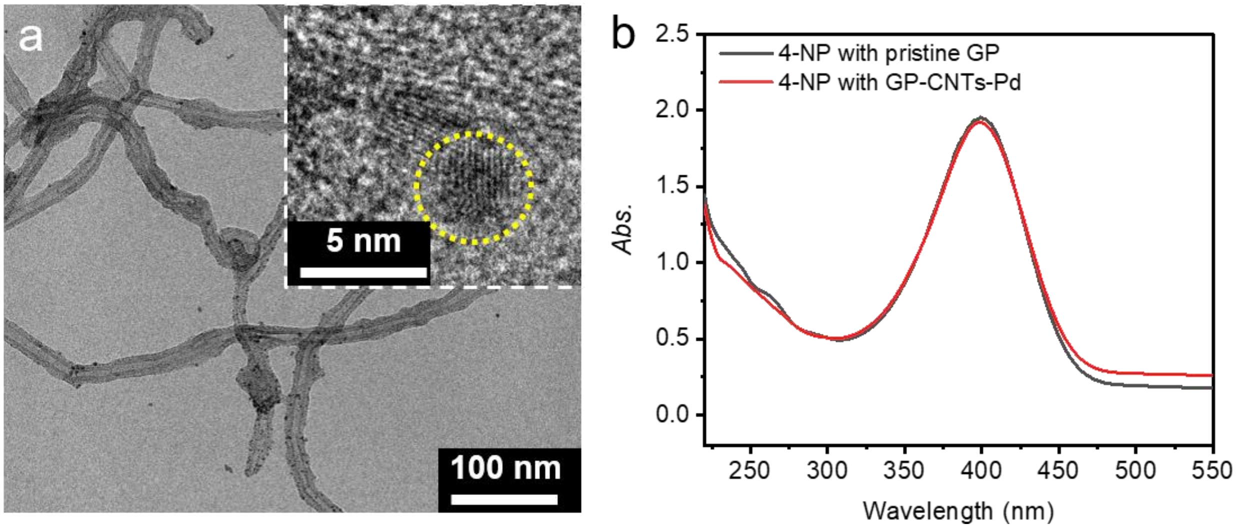

Fig. S18. (a) TEM image of the GP-CNTs-Pd dispersion after catalytic cycles. (b) Reduction reaction of 4-NP with either GP-CNTs-Pd or pristine GP molecules at pH of ~10 without $NaBH_4$ after 15 min.

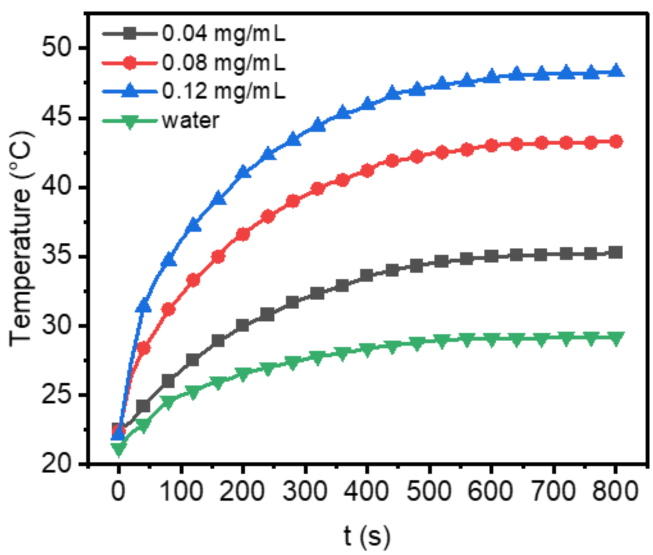

Fig. S19. Temperature variation of the GP-CNTs-Pd dispersion at various concentrations.

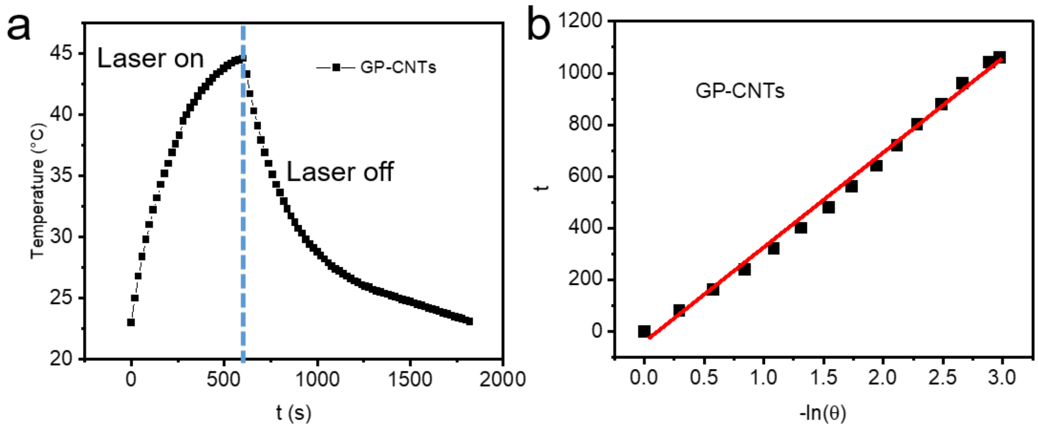

Fig. S20. (a) Temperature variation of the GP-CNTs dispersion under NIR irradiation. (b) *t* versus *–ln(θ)* obtained from the cooling curve.

The photothermal conversion efficiency (η) can be calculated based on the heating-cooling profiles and given by:

$$\eta = \frac{hs(T_{max} - T_{sur}) - Q_{Dis}}{I(1 - 10^{A_{808}})} \qquad (2)$$

where *h*, *s*, Q_{Dis}, are the heat transfer coefficient, surface area of the container, heat dissipated from the light absorbed by the quartz sample cell containing with pure water, respectively. *I* and A_{808} are the laser intensity and absorption of dispersion at the wavelength of 808 nm, respectively. where T_{sur}, T_{max} are surrounding temperature and maximum temperature of the GP-CNTs dispersion, respectively.[4, 5]

To calculate *hs*, a dimensionless parameter (θ) needs to be introduced and determined by:

$$hs = \frac{m_D C_D}{\tau_s} \qquad (3)$$

where m_D and C_D are the mass of water (1 g) and heat capacity (4.2 J/g·°C), respectively. The time constant (τ_s) can be determined from the slop of cooling curve (**Fig. S16b**) according to the equations below:

$$t = -\tau_s \ln(\theta) \qquad (4)$$

$$\theta = \frac{T - T_{sur}}{T_{max} - T_{sur}} \qquad (5)$$

where t and T are the time and cooling temperature of the dispersion during cooling stage. Hence, τ_s of the pristine CNTs cluster and GP-CNTs dispersion were determined to be 328.1 and 370.4 s, respectively. Correspondingly, the value η of CNTs cluster and the GP-CNTs dispersion were determined to be 4.2 % and 22.3 %, respectively.

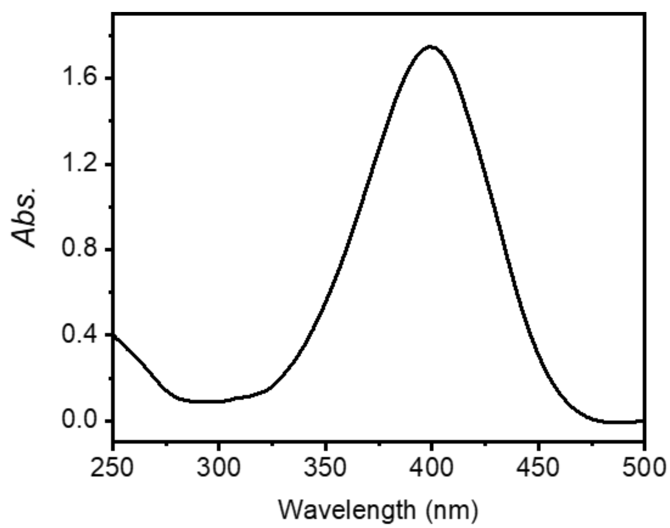

Fig. S21. Reduction reaction of 4-NP after NIR light irradiation for 15 min before introducing $NaBH_4$.

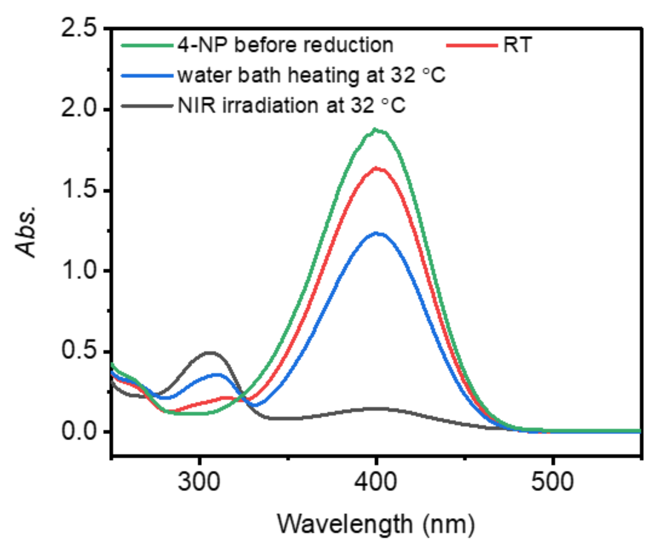

Fig. S22. Reduction reaction of 4-NP under various heating conditions after 5 min.

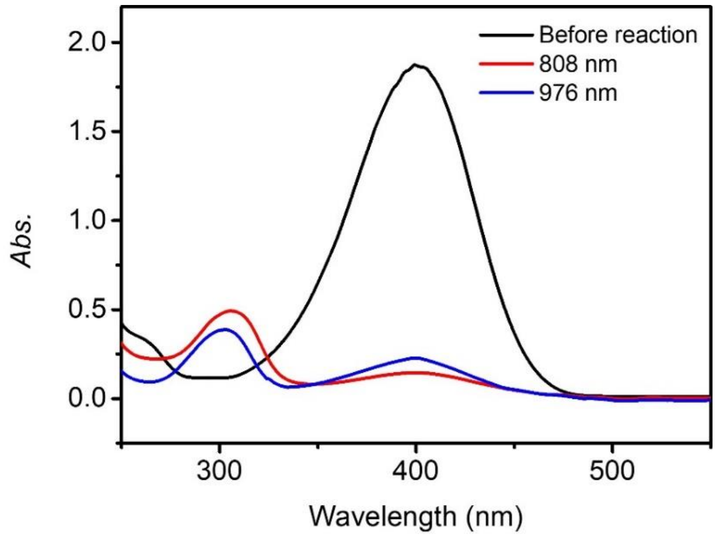

Fig. S23. Reaction comparison of GP-CNTs-Pd under NIR light illumination at 808 and 976 nm (3 W/cm^2) for 5 min with the concentration of GP-CNTs-Pd at 0.03 mg/mL, 4-NP at 1 mM, and $NaBH_4$ at 0.2 M.

Supplementary Tables

Table S1. Comparison of the catalytic activity of the Pd-based catalysts.

Sample	**Size (nm)**	$C_{cat.}$	C_{NaBH4} **(mM)**	$C_{4\text{-}NP}$ **(mM)**	***t*** **(min)**	***T*** **(°C)**	$k_m \times 10^{-3}$ s^{-1} mg^{-1}	**Ref.**
Pd-peptide	2.6	79 µM	10	0.05	10	25	8.73	6
Pd	26.5	5 µg/mL	100	2	20	25	24	7
Pd-Au/PS-PVP	3.1	3.6 µg/mL	20	0.1	10	25	95.6	8
Pd/protein	2.8	0.6 mg/mL	10.5	0.1	10	20	3.33	9
Pt-Pd alloy	~57	5 µg/mL	100	0.1	10	22	226.7	10
Pd-PAMAM	1.8	0.01 mM	10	0.2	15	15	113.3	11
GP-CNTs-Pd	1.8	50 µg/mL	20	0.1	10	25	146.5	This work

Note that C_{cat}, C_{NaBH4}, $C_{4\text{-}NP}$, t, T, and k_m are the catalyst concentration, $NaBH_4$ concentration, 4-NP concentration, reaction time, reaction temperature, and k_{app} normalized with the catalyst mass, respectively.

Table S2. Summary for the calculation of S_t.

Metal	m **(µg)**	ρ **(g/cm³)**	d **(nm)**	m_0 **(g)**	n	S_0 **(m²)**	S_t **(m²/L)**
Pd	0.59	12.0	1.8	3.66×10^{-20}	1.61×10^{13}	4.07×10^{-17}	0.26
Au	3.02	19.3	5.6	1.77×10^{-18}	1.70×10^{12}	3.93×10^{-16}	0.26

References in SI:

1. S.-H. Min, G.-Y. Lee and S.-H. Ahn, *Composites Part B: Engineering*, 2019, **161**, 395-401.
2. S. Wunder, F. Polzer, Y. Lu, Y. Mei and M. Ballauff, *J. Phys. Chem. C*, 2010, **114**, 8814-8820.
3. P. Hervés, M. Pérez-Lorenzo, L. M. Liz-Marzán, J. Dzubiella, Y. Lu and M. Ballauff, *Chem. Soc. Rev.*, 2012, **41**, 5577-5587.
4. X. Liu, B. Li, F. Fu, K. Xu, R. Zou, Q. Wang, B. Zhang, Z. Chen and J. Hu, *Dalton Trans.*, 2014, **43**, 11709-11715.
5. G. M. Neelgund and A. Oki, *Ind. Eng. Chem. Res.*, 2018, **57**, 7826-7833.
6. R. Bhandari and M. R. Knecht, *ACS Catalysis*, 2011, **1**, 89-98.
7. N. K. Reddy Bogireddy, K. K. H. Anand and B. K. Mandal, *Biointerface Res. Appl. Chem.*, 2018, **8**, 3319-3323.
8. S. Mei, J. Cao and Y. Lu, *J. Mater. Chem. A*, 2015, **3**, 3382-3389.
9. S. Behrens, A. Heyman, R. Maul, S. Essig, S. Steigerwald, A. Quintilla, W. Wenzel, J. Bürck, O. Dgany and O. Shoseyov, *Adv. Mater.*, 2009, **21**, 3515-3519.
10. Y. Wang, Q. Li, P. Zhang, D. O'Connor, R. S. Varma, M. Yu and D. Hou, *J. Colloid Interface Sci.*, 2019, **539**, 161-167.
11. K. Esumi, R. Isono and T. Yoshimura, *Langmuir*, 2004, **20**, 237-243.